Numerical simulations of the ice flow dynamics of Fimbulisen

Angelika Humbert[1]

[1]*Section Mechanics, Department of Mechanical Engineering, Darmstadt University of Technology, Hochschulstraße 1,D-64289 Darmstadt, Germany*
humbert@mechanik.tu-darmstadt.de

Abstract

A diagnostic, dynamic/thermodynamic ice-shelf model is applied to Fimbulisen, which is situated in the Haakon VII Sea, Antarctica. Fimbulisen is characterized as an unbounded ice shelf with one main inflow, the ice stream Jutulstraumen.

We simulate the present ice flow over the ice shelf that results from the ice-thickness distribution, the inflow at the grounding line and the surface and bottom temperature. Particular focus are different vertical ice temperature profiles, that are indicated by basal melting and the measured temperature profile at the drill hole S1. Furthermore, shear zones were included, supporting lateral shear margins of the Jutulstraumen.

We also assessed the model's sensitivity to ice thickness, inflow velocities, the ice temperature profile and a flow enhancement factor. The latter is representing the mechanical properties of the ice in the shear margins.

1 Introduction

Ice shelves are sensitive elements of the climate system and govern to a large extent the mass loss of the inland ice which they bound. It is therefore important to understand their dynamics, how ice shelves react to external conditions such as thickness and temperature distributions, boundary conditions of ice inflow from the inland ice, outflow to the ocean at the front and reactions to pinpointing ice rises. The equations of the Shallow Shelf Approximation (SSA) are non-linear elliptic equations, requiring boundary conditions to be imposed along all boundaries and transmitting a localized boundary effect over all points of the ice shelf. The equations do, however, not disclose, how strong these far field effects are and how far a boundary feature propagates to generate measurable values for physical observables.

In this paper an attempt is made to shed some light on these questions using Fimbulisen as a test case. We shall demonstrate that the temperature field and the thickness distribution are parameter fields to which the ice shelf reacts conspicuously, that the order of magnitude of the rate factor in Glen's flow law is equally important, but that changes in the inflow boundary conditions seem to have a lesser significance.

A second aim of this paper is to validate the model equations by comparing computed results with corresponding field data. Whilst thickness distributions and flux boundary conditions are observational input data fraught with their own errors, velocities at interior ice-shelf points are used as comparison points to test the validity of the model. In practice, the density of such points is extremely dilute - sometimes only data at one or two isolated points are known - implying that verification of the model is on rather shaky grounds. This will be demonstrated in this paper. The computations show that completely different parameter identifications for the input quantities generate fields for observables that can not be separated from one another by a failure criterion of matching/not matching corresponding observational data. This result demands for more theoretical complexity, implying higher resolution in the data as well, a fact which data collectors and analysts may may have difficulty to provide.

2 Fimbulisen

Fimbulisen, an ice shelf bounding Dronning Maud Land, Antarctica, is located from 71.5°S to 69.5°S and 3°W to 4°E and has an approximate size of 36.505 km^2 with a floating part of 33.209 km^2. It is the largest ice shelf in the Haakon VII Sea. Its morphology has been studied by Swithinbank (1957) and Lunde (1961) (see Fig. 1). The Jutulstraumen ice stream, the largest outlet glacier in Dronning Maud Land, feeds the central part of the ice shelf. The inflow of this large ice stream builds up an ice tongue inside the ice shelf, the Trolltunga, which divides the ice shelf in a fast moving inner part and a slow moving surrounding part. The shear zone between the different ice masses is visible in satellite images as a highly crevassed area. The crevasses form canyons up to 100 m wide, partly even with access to open water (private communication Ole Anders Nøst, 2004). Trolltunga also marks the northern margin of the ice shelf and is the only ice shelf extending further than the continental shelf, which is the Haakon VII Sea closest to the inland ice margins all around the Antarctic coast. This makes Fimbulisen special, since the water masses draining under the ice shelf are different to those from e.g. the Ross Ice Shelf (Humbert et al., 2005). Fimbulisen includes a number of ice rises, which partly mark their sideward margins. The sizes of the ice rises range from very small, even unnamed rises with areas as small as 15 km^2, east of the Blåskimen Ice Rise at the ice front, to ice rises with sizes of about 1180 km^2, like the Blåskimen Ice Rise. An overview of the ice shelf is given in Fig. 1.

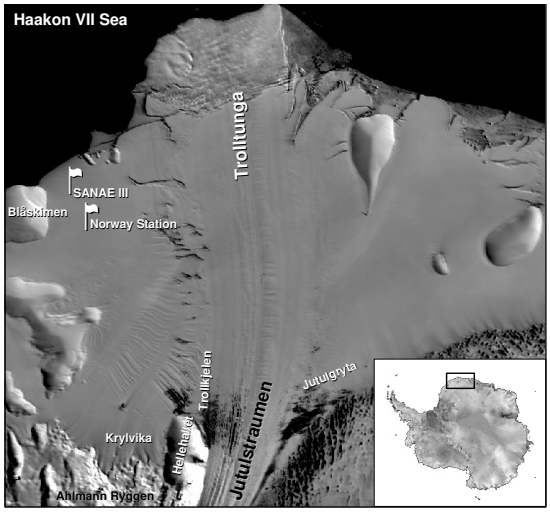

Figure 1: MODIS image of Fimbulisen, Jutulstraumen, Dronning Maud Land and Haakon VII Sea, showing locations mentioned in the text.

Two stations were located on Fimbulisen: the South African station "SANAE III" and the Norwegian station "Norway" (see Fig. 1). The current South African Station, SANAE IV is on grounded ice.

Ice thickness measurements have been performed as early as 1951-52 by means of seismic shootings performed by the Norwegian-British-Swedish Antarctic expedition. The data are shown in Fig. 2(right panel). They were taken at 44 points from 71.9°S to 71.1°S and 8.9°W to 4.7°W (this is outside our modelling domain). This was followed by the 1968-69 Belgian Antarctic Expedition, which took radio echo soundings at 751 data points in the western area of Fimbulisen, between Blåskimen Ice Rise and Trolltunga. These data are also shown in Fig. 2(right panel). During austral summer 1994-95 the Alfred Wegener Institute carried out a campaign using airborne radio echo sounding. The coverage was an area of 948 000 m^2 in the western and central Dronning Maud Land, with one crossing of Fimbulisen and two flight lines along both sides of the grounding line (Steinhage et al., 1999). On Fimbulisen (in our modelling domain) data at 5106 data points were recorded; they are shown in the left panel of Fig. 2(middle panel). In the 2000-01 field season the ice thickness was measured by means of seismic shooting by the Norwegian Antarctic Research Expedition in a wide area that covered almost the whole Fimbulisen (Nøst et al., 2002; Nøst, 2004). The data were taken at 169 locations with an almost constant data density over the whole ice shelf, like a grid. The aquired ice thickness data is shown in the right panel of Fig. 2(left panel).
The ice thickness ranges from by means of seismic shooting minimum of 144 m to a maximum of 790 m, taking into account all measured data inside the modelling domain.

At position 70°58.72'S, 0°11.93'E with 53 m elevation a hot water drill was performed in 1990 (Orheim et al., 1990a,b), with the purpose to obtain an access hole to the sea. This drill location named S1, will subsequently frequently be referred to. The ice at that location was 399±1 m thick. Near the base of the ice shelf, the water level in the drill hole rose immediatly to 45 m. This is an indication that, throughout the depth, the ice consisted of solid meteoric ice. At the drill on the Amery Ice Shelf (Craven et al., 2003) and at the J9 drill on the Ross Ice Shelf (Zotikov, 1979; Zotikov et al., 1980), the water level rose much before the bottom of the ice was penetrated. Both drills contained a certain amount of marine ice at the bottom. In the drill hole on Fimbulisen a thermistor string was frozen. The temperature was recorded by sensors in 2, 7, 12, 17, 22 and 27 m depth and then at every 25 m down to 327 m (∼81% of the depth). The temperature profile, obtained in read-outs a year after the string was installed, shows an unusual bevaviour. The temperature decreases from the ice-atmosphere transition towards the bottom; at about 80% of the depth the ice is approximately 10°C colder than on the surface. Assuming that the temperature profile is representative for a large area of the ice shelf this means, that the amount of cold ice is much larger than in other ice shelves.

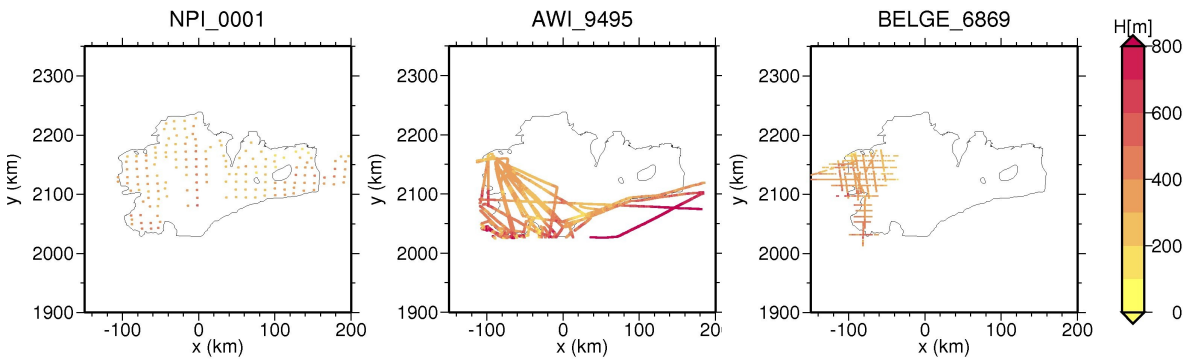

Figure 2: Left panel: Ice thickness data measured during the Norwegian Antarctic Research Expedition 2000-01. Middle panel: Data collected during the campaign of the Alfred Wegener Institute 1994-95. Measurements were done by means of airborne radio echo sounding. Right panel: Ice thickness data in western Fimbulisen obtained by the 1968-69 Belgian Antarctic Expedition.

At Jutulgryta, a drill through the very thin (∼38 m thick) ice was made in February 1990, giving access to the water cavity beneath the ice, so that vertical CTD profiles could be obtained (Orheim et al., 1990a,b). This thin floe was surrounded by ice of a thickness between 200 and 300 m. The CTD profiles showed a three layered structure of the water masses. The uppermost layer, approximately 40-50 m thick, shows a clear manifestation of melting beneath the ice; the layer has temperatures close to freezing of sea water at low salinity. The middle layer, from 50 to 300 m exhibits stable temperatures and salinities with a range of 70 m supercooled water masses at the beginning of the layer. Below 300 m the salinity and temperature increase, most likely because the connection between this layer and the sea water outside the ice shelf is better. Overall, these CTD measurements suggest, that Fimbulisen is, a melting type ice shelf at least in the vicinity of Jutulgryta. Therefore, simulations shall also be done with a melting type temperature profile. The data is shown in Fig. 3 in red colour.
Melvold et al. (1997) report data from a shallow drill at 70°45'S, 0°1'E down to a depth of 30.1 m, named Core K. The data is shown in Fig. 3 in green colour. As S1, Core K shows the same tendency of decreasing temperature with increasing depth.

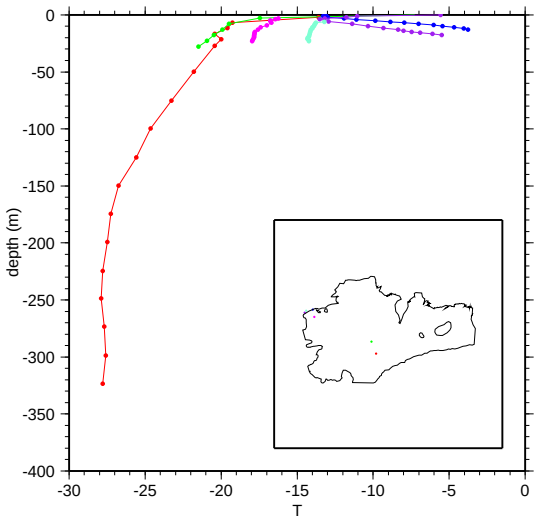

Figure 3: Measured temperature profiles of Fimbulisen. Inset shows the locations of the drills.

In the 60's, a series of shallow drills was carried out, all relatively close to the ice front (du Plessis, 1973). The temperature profiles exceed the 10 m depth in only a few of these drill holes. One drill was made 3 km from the ice front, half-way between the small ice rises and Blåskimen Ice Rise in valleys leading into bays, with a depth of 18 m, where the surface elevation was 23 m (∼202 m ice thickness of which ∼8% were drilled through). The temperature profiles show the tendency of warming with depth, with a *steady near-linear temperature increase of 0.66° C per meter, which would indicate -2.0° C at 22 m. In this case also brine would be expected to occur at sea-level*(du Plessis, 1973). It is unlikely, that the slope of the linear profile is really steady, indeed a change in slope might occur to reach the freezing temperature of sea water at the bottom of the ice. However, these temperature profiles definitely undermine the assumption that the trend of S1 is a general trend for the whole ice shelf. The profiles from other drills displayed in Fig. 3, show that even within small distances the trend is different. These results make extrapolation to an ice-shelf temperature field extremly conjectural since only two regions are covered: one site directly at the ice front and one in the fast middle part of the ice shelf.

3 The model

A three-dimensional, thermodynamical consistent dynamic model for ice shelf flow was developed by Weis (2001), using a general, continuum mechanical approach. Here, we solve diagnostically the elliptic boundary-value problem for the horizontal velocity in the shallow-shelf approximation (SSA). The deformation of ice is described by Glen's flow law (e.g. Paterson, 1994),

$$\boldsymbol{D} = EA(T)f(\sigma)\,\boldsymbol{t}^{\mathrm{D}}, \quad \text{with } f(\sigma) = \sigma^{n-1},\ n = 3, \tag{1}$$

where $\boldsymbol{D} = \operatorname{sym}\operatorname{grad}\boldsymbol{v}$ is the strain-rate tensor [symmetric part of the gradient of the velocity $\boldsymbol{v} = (v_x, v_y, v_z)$], $\boldsymbol{t}^{\mathrm{D}}$ the Cauchy stress deviator, $\sigma = [\mathrm{tr}\,(\boldsymbol{t}^{\mathrm{D}})^2/2]^{1/2}$ the effective stress, n the stress exponent, T the absolute temperature, $A(T)$ the flow-rate factor (see below) and E the flow enhancement factor.

Insertion of the flow law (1) in the SSA limit of the horizontal force balance yields the elliptic differential equations for the horizontal velocity (v_x, v_y) (see Weis et al., 1999),

$$\begin{aligned}
2\frac{\partial}{\partial x}\left(\bar{\nu}\frac{\partial v_x}{\partial x}\right) + \frac{\partial}{\partial x}\left(\bar{\nu}\frac{\partial v_y}{\partial y}\right) + \frac{1}{2}\frac{\partial}{\partial y}\left[\bar{\nu}\left(\frac{\partial v_x}{\partial y} + \frac{\partial v_y}{\partial x}\right)\right] &= \varrho H\frac{\partial H}{\partial x} + \frac{\tau_x^{\mathrm{d}}}{\rho g},\\
\frac{\partial}{\partial y}\left(\bar{\nu}\frac{\partial v_x}{\partial x}\right) + 2\frac{\partial}{\partial y}\left(\bar{\nu}\frac{\partial v_y}{\partial y}\right) + \frac{1}{2}\frac{\partial}{\partial x}\left[\bar{\nu}\left(\frac{\partial v_x}{\partial y} + \frac{\partial v_y}{\partial x}\right)\right] &= \varrho H\frac{\partial H}{\partial y} + \frac{\tau_y^{\mathrm{d}}}{\rho g},
\end{aligned} \tag{2}$$

where the coordinates x and y span the horizontal plane, $\bar{\nu}$ is the effective viscosity, $\varrho = (\rho_{\mathrm{sw}} - \rho)/\rho_{\mathrm{sw}}$ the relative density (ρ_{SW}: density of sea water ($1028\,\mathrm{kg\,m^{-3}}$), ρ_{ice}: density of meteoric ice ($910\,\mathrm{kg\,m^{-3}}$)), H the ice thickness, g the gravity acceleration, and $\tau_{x,y}^{\mathrm{d}}$ the basal drag in the x and y directions. The latter is set to zero for the floating ice shelf, but can be assigned non-vanishing values for grounded ice rumples (not done in this study). For the effective viscosity,

$$\bar{\nu} = \frac{1}{\rho g} d^{\frac{1-n}{n}} \int_{h_{\mathrm{b}}}^{h_{\mathrm{s}}} E_{\mathrm{s}} B(T)\, dz, \tag{3}$$

where z is positive upward, $E_{\mathrm{s}} = E^{-1/n}$ is the stress enhancement factor, $B(T) = [A(T)]^{-1/n}$ the associated rate factor, h_{s} and h_{b} are the positions of the free surface and the base (ice-ocean interface), respectively (ice thickness $H = h_{\mathrm{s}} - h_{\mathrm{b}}$), and

$$d = \sqrt{\left(\frac{\partial v_x}{\partial x}\right)^2 + \left(\frac{\partial v_y}{\partial y}\right)^2 + \frac{\partial v_x}{\partial x}\frac{\partial v_y}{\partial y} + \frac{1}{4}\left(\frac{\partial v_x}{\partial y} + \frac{\partial v_y}{\partial x}\right)^2} \tag{4}$$

is the effective strain rate (second invariant of the strain-rate tensor). For the associated rate factor $B(T)$, the relation by Hooke (1981) is employed,

$$B(T) = B_0 \exp\left(\frac{T_0}{T} - \frac{C}{(T_{\mathrm{r}} - T)^k}\right), \tag{5}$$

with the parameters $B_0 = 6.984 \times 10^{-6}\,\mathrm{kPa\,s^{1/3}}$, $T_0 = 3155\,\mathrm{K}$, $T_{\mathrm{r}} = 273.39\,\mathrm{K}$, $k = 1.17$ and $C = 0.16612\,\mathrm{K}^k$.

The elliptic system of differential equations (2) is subject to two different types of boundary conditions: (i) Inflow of ice along the grounding line from the adjacent inland ice, and (ii) a vertically integrated stress boundary condition at the front edge. Further, the ice-thickness distribution $H(x, y)$ and the temperature field $T(x, y, z)$ must be prescribed.

The C^{++} program FESSACODE solves the above boundary-value problem by employing the finite element technique. Numerical determination of the velocity field is accomplished by an iterative integration procedure. This iteration is needed because of the non-linear flow law (1) and encompasses a sequential updating of the effective viscosity (3). The performance of FESSACODE was verified by applying it to a simple, "academic" problem for which an exact analytical solution exists (Weis, 2001).

4 Simulation set-up: input quantities

4.1 Boundary: grounding line and ice front

For the grounding line and the ice front, a dataset kindly provided by Ole Anders Nøst was used. The triangulation resulted in 2269 nodes. In comparison to the Ross Ice Shelf (see Humbert et al., 2005) the

margins of Fimbulisen are extremly fine-structured and frayed, as visible in Fig. 1. To keep the amount of nodes in a triangulated mesh within an acceptable range, the polygon of the margin has been slightly smoothed. Nevertheless, the number of nodes could not substantially be reduced. Thus, the computing time is still dramatic. This is particulary so because the number of iterations to conform with Glen's flow law has been set to 50, which garantees convergence. Special setups, including shear zones and the resulting larger number of nodes are discussed later.

4.2 Ice thickness

The ice thickness data described above was used to determine an ice thickness grid. To estimate the difference using the data with and using the data from the overflight lines, two thickness grids were evaluated. Both are shown in Figure 4. The left panel shows the thickness grid using the GMT (http://gmt.soest.hawaii.edu/) surface algorithm without the AWI data, the right panel displays the determined grid using all thickness data. The thickness data obtained by airborne radio-echo soundings show strong variations even inside flight lines. These thickness variations likely occur because of shear zones and rifts in the ice shelf. In simulations large variations on small scales lead to large velocity variations, since the gradient of the thickness acts as a driving force in the equations. To avoid unrealistic velocities, the thickness grid, using the data of the airborne radio-echo soundings, has been determined with a rougher resolution. Both grids reflect the inflow of Jutulstraumen very well. In the right panel, the Trolltunga is more pronounced and more narrow than in the left panel. Without the AWI data, the inflow area of Jutulstraumen shows almost only northward gradients.

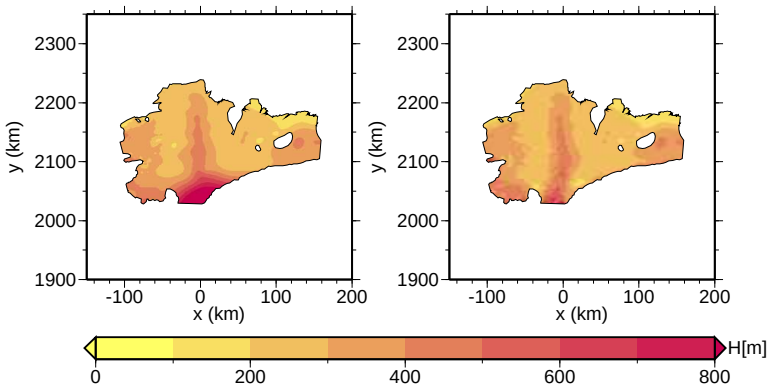

Figure 4: Left panel: Ice thickness grid derived taking into account all thickness data except those from the airborne radio echo sounding. Right panel: Ice thickness grid taking all measurements into account.

4.3 Inflow velocity

The inflow velocity was taken from measurements of a profile at the flow gate of Jutulstraumen performed by Melvold et al. (1997), and set for the simulations to 720 $\mathrm{m\,a^{-1}}$with a bearing of 270°. At the remainder of the grounding line between inland ice and shelf ice along Ahlman Ryggen and Hellehallet (Fig. 1) zero flux was assumed. Outflow from ice rises was set to zero as well.

Tremendous difficulties arose in finding velocity measurements on the ice shelf for comparison of the results. The only stake measurements were performed by Orheim et al. (1990a) at S1. There the velocity was detected to be 720 $\mathrm{m\,a^{-1}}$.

Of the former SANAE station, SANAE III, an emergency base (E-Base) is still in use for unloading ships. The current overwintering team recorded waypoints by means of GPS. During a second visit with bad weather conditions they recognised problems in finding the E-Base at the location formerly determined. The base moved by approximately 260 m (Beneke de Wet, pers. comm.).

The velocity at the ice front is mentioned once to be in the order of 2000 $\mathrm{m\,a^{-1}}$(Orheim and Lucchitta, 1987). Very likely, this value was estimated from satellite images taken at different times. This is, however, not recording the material velocity of the ice, but rather that of the icefront. This can only be assumed to be the same in case of **no** calving. Calving is very likely taking place at Fimbulisen, and there is no argument saying that it cannot take place.

4.4 Temperature regime

From the temperature profiles discussed above and the oceanographic investigations performed by Orheim et al. (1990a) and Nøst and Foldvik (1994) we cannot coherently conclude about the accumulation type of the ice shelf. Oceanographic arguments claim Fimbulisen to be a melting type ice shelf. This would give reason for a parabolic or linear temperature-depth relation. For the simulations we decided to run three different scenarios: i) assuming strong melting and therefore a parabolic temperature profile; ii) assuming moderate melting suggesting a linear profile and iii) parameterising the temperature as a set of two linear relations analogous to the measured profile at S1, which we subsequently shall call S1-like temperature profile. The shape of these temperature profiles is displayed in Fig. 5. In order to derive profiles applicable to the entire ice shelf, we define a normalized vertical coordinate ζ and a normalized temperature Θ by

$$\begin{aligned} \zeta &= -\tfrac{h_\mathrm{s}-z}{h_\mathrm{s}-h_\mathrm{b}}, \\ \Theta &= -\tfrac{T_\mathrm{b}-T}{T_\mathrm{b}-T_\mathrm{s}}, \end{aligned} \tag{6}$$

so that $\zeta = 0$ corresponds to the ice-shelf surface, $z = h_\mathrm{s}$, $\zeta = -1$ to the ice-shelf base, $z = h_\mathrm{b}$, $\Theta = -1$ to the surface temperature $T = T_\mathrm{s}$ and $\Theta = 0$ to the basal temperature, $T = T_\mathrm{b}$. The latter is assumed to be equal to the freezing temperature T_f of the ocean water below the ice shelf,

$$T_\mathrm{f} = -0.036 - 0.00759\,P - 0.0499\,S - 0.000112\,S^2, \tag{7}$$

where T_f is in °C, P is the hydrostatic pressure in bar and S the salinity in ppt (Fujino et al., 1974). For the latter we use the fixed value $S = 34.6$ ppt.

The linear temperature profile is defined as

$$\Theta(\zeta) = -\zeta - 1, \tag{8}$$

the parabolic temperature profile is described by

$$\Theta(\zeta) = a\zeta^2 + (a-1)\zeta - 1, \tag{9}$$

and for the simulations a is set equal to 1.

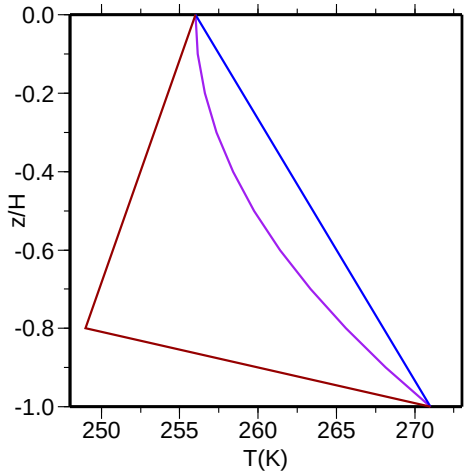

Figure 5: Three different parameterisations for the temperature profile. The linear law (blue) represents moderate melting, the parabolic (purple) curve represents strong melting and the dark red curve is a parameterisation of the measured profile.

For the parameterisation of the S1-like profile we implemented two representations based on the measured temperature profile: i) the profile consists of two linear functions; ii) a maximum temperature inversion of 7°C is reached at 80% depth (ζ=-0.8). With the corresponding normalized temperature Θ_{const}, we obtain

$$\Theta(\zeta) = \begin{cases} -1.25(1+\Theta_{const})\zeta - 1, & \forall \zeta \geq -0.8, \\ \\ 5\Theta_{const}(\zeta + 1.0), & \forall \zeta < -0.8. \end{cases} \tag{10}$$

The surface temperatures are set equal to a constant. There is no Automatic Weather Station on the Fimbulisen. Therefore an average of the 10 m temperature, obtained by du Plessis (1973), was used. This corresponds to a surface temperature of -17°C .

4.5 Enhancement factor

The simulations were run at a first step with an enhancement factor of E_s= 1.0 for all three temperature parameterisations. For the linear and parabolic temperature profile in a second step E_s was set equal to a value of 0.84, because this value was obtained in simulations of the Ross Ice Shelf. Finally, for each parameterisation the enhancement factor was adjusted such that the simulated velocity at position S1 and the measured velocity showed best agreement.

5 Results

5.1 Role of the Ice Thickness Distribution

To investigate the influence of the ice thickness distribution to the horizontal velocities, we ran simulations with an assumed linear temperature profile and for E_s =1.0. The inflow at the grounding line was assumed

along the inflow gate of Jutulstraumen with a magnitude of 720 ma^{-1}. As the data evaluation has a chronological structure, so had our first runs of the simulations. They were primarily carried out with the thickness grid 'NPI' shown in Fig. 4. This thickness distribution is structurally typified by a large gradient to the north and to both sides of the inflow of Jutulstraumen. As can be seen in Fig. 6, this gradient pushes the ice tremendously so that horizontal velocities even above 2000 $ma^{-1}$are reached close to the inflow gate of Jutulstraumen at the grounding line. Since the velocity at S1 is as large as 720 ma^{-1}we estimate the ice thickness gradient to be too high. (Notice that a value of E_s smaller than 1 will lead to higher horizontal velocities.)
The ice thickness grid 'AWI' (shown in Fig. 4), which is based on the present complete set of ice thickness data, is used for the second simulation. The results are shown in the right panel of Fig. 6. In comparison with the left panel a dramatic decrease of the velocity can be seen. This is due to the decreased ice thickness gradient along the inflow gate of Jutulstraumen. However, the structure of the fast middle part is still well represented. With 448 $ma^{-1}$the velocity at S1 is 38% too low, but still of an acceptable value, in particular if it is kept in mind, that the linear temperature profile and E_s are only guesses.

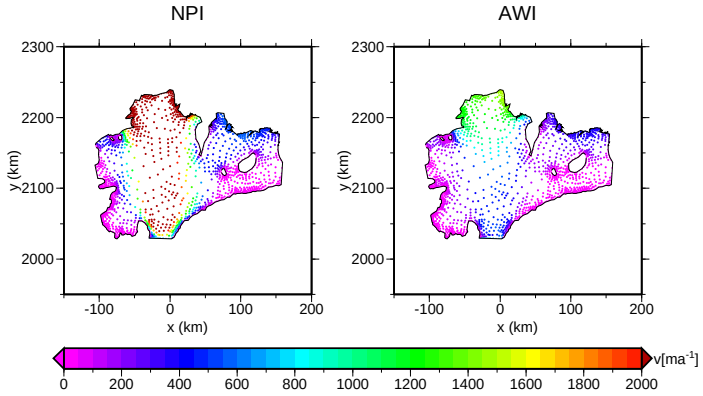

Figure 6: Left panel: simulated horizontal velocity distribution using the thickness grid NPI (see left panel, Fig.4) Right panel: simulated horizontal velocity distribution using the thickness grid AWI (see right panel Fig.4).

Such a close presentation of the flow lines of an ice stream could so far not be reached for any other ice shelf and is therefore a remarkable step in the development of simulations of the flow of an ice shelf. The reason is likely the ice thickness grid that represents the real ice thickness and the gradients well. Therefore, a general main focus of investigation shall lie in the estimation of the ice thickness distribution of ice shelves.

5.2 Role of the Inflow Velocity

Investigations about the role of the influence of the inflow velocity are rudimentary and divide between the inflow that could be estimated to be most realistic and no inflow. For comparison, model setups using the thickness grid 'AWI', a linear temperature profile and E_s =1.0 were chosen. Fig. 7(left panel) shows a scenario without inflow and Fig. 7(right panel) displays one with an inflow of magnitude 720 $ma^{-1}$and a bearing of 270°. The velocity at S1 was reduced to 317 ma^{-1}in comparison to 448 $ma^{-1}$with an inflow, which is about 30%. Using the thickness distribution 'NPI', the difference is only 11% (results not shown). This leads to the conclusion that propagation of the inflow velocity on the ice shelf is coupled with the ice thickness gradient. In case the ice thickness gradient is dominating the ice flow, the inflow has less influence. In simulations of the Ross Ice Shelf (Humbert et al., 2005) we could see that the inflow did not propagate far from the grounding line. Compared to our results of Fimbulisen, the conclusion can be, that the inflow can only propagate if the ice thickness grid is not hindering it.

5.3 Linear Temperature Profile

Simulations of this section were done with a linear temperature profile. Furthermore, the ice thickness grid 'AWI' was used and an inflow as described above. The simulations were performed for several values of E_s, including E_s = 0.84, the value that was derived in simulations of the Ross Ice Shelf (see Humbert et al., 2005). Results for E_s = 0.84 are displayed in Fig. 8(left panel); they should be contrasted with those of Fig. 7(right panel), which holds for E_s =1.0.

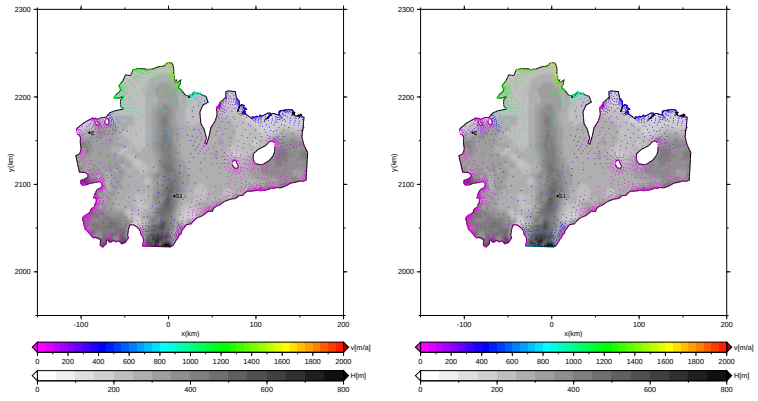

Figure 7: Left: Horizontal velocity distribution assuming no inflow. Right: Horizontal velocity distribution assuming an inflow exclusively at the inflow gate of Jutulstraumen of 720 $\mathrm{ma}^{-1}$and a bearing of 270°. The colour refers to the magnitude of the velocity. Underlying is the ice thickness distribution. More setup details: Ice thickness grid'AWI', linear temperature profile and $E_s = 1.0$. The symbols E and S1 mark measuring stations for the velocity.

5.4 Parabolic Temperature Profile

A parabolic temperature profile is the focus of this section. Figure 8(middle panel) shows the resulting horizontal velocity distribution obtained with $E_s = 1.0$.

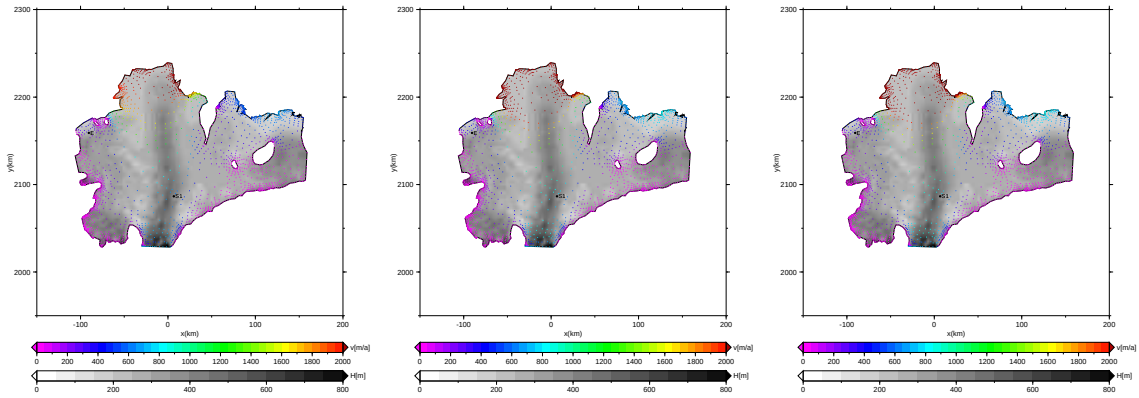

Figure 8: Left: Horizontal velocity distribution assuming a linear temperature profile and $E_s = 0.84$. Middle: Horizontal velocity distribution assuming a parabolic temperature profile and $E_s = 1.0$. Right: Horizontal velocity distribution assuming a parabolic temperature profile and $E_s = 0.7$. The colour denotes the magnitude of the velocity. More setup details: ice thickness grid 'AWI', inflow exclusively at the inflow gate of Jutulstraumen of 720 $\mathrm{ma}^{-1}$and a bearing of 270°.

The best agreement could be reached with $E_s = 0.7$ that is shown in Fig. 8(right panel). This value is slightly less than that for the linear case. The structure of the velocity distribution with an accelaration towards the ice front is represented well.

5.5 S1-like Temperature Profile

The simulations of this section are supposed to be the most realistic ones, since they use the S1-like temperature profile, assuming this to be representative for the whole ice shelf. Apart from the temperature profile all other input quantities are the same as for the linear and parabolic profile. For the first run E_s is set equal to 1.0. As expected the horizontal velocity is now much reduced. At S1 the velocity is now only 4.8 ma^{-1}. This is much too low, representing an ice shelf that is motionless.

Therefore, E_s was chosen such that the velocity at S1 matches with that, which was measured. This could be achieved with E_s =0.15 (Fig. 9), which leads to a horizontal velocity at S1 of 753 ma^{-1}, a value

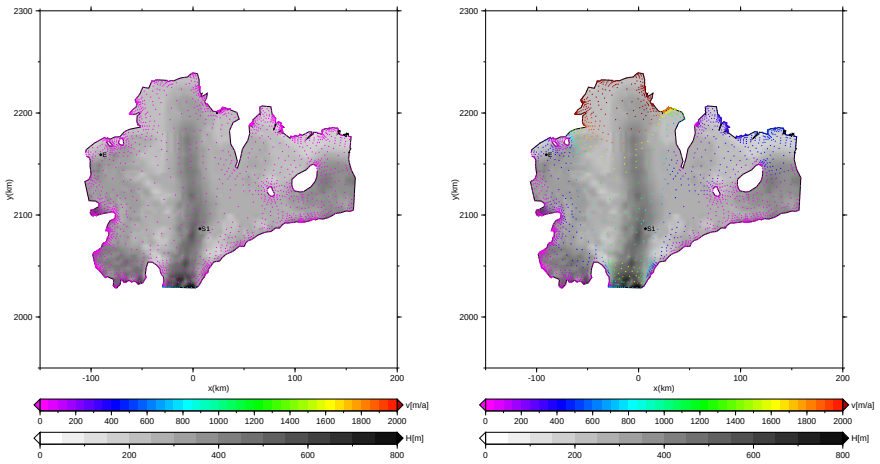

Figure 9: Horizontal velocity distribution assuming a S1-like temperature profile and E_s =1.0 (left panel) and E_s =0.15 (right panel). The colour denotes the magnitude of the velocity. More setup details: Ice thickness grid 'AWI', inflow exclusively at the inflow gate of Jutulstraumen of 720 $\mathrm{m\,a^{-1}}$and a bearing of 270°

that is extremly low and likely unrealistic. We have, of course, no possibility to prove that a value of 0.15 is unrealistic, since there might be a composition of polycrystalline ice, that justifies this value, like e.g. in shear zones. Interesting, however, is the fact that the structure of the horizontal velocity distribution over the whole ice shelf is far less uniform than in Fig. 9(left panel), but resembles that of Fig. 8(right panel).

5.5.1 S1-like Temperature Profile with Shear Zones

As discussed above, Fimbulisen shows areas of shear zones. These zones can physically not be described by the same enhancement factor as *undisturbed* ice. The difficulties of obtaining realistic horizontal velocities with the S1-like temperature profile led to the application of zones in which the enhancement factor was chosen differently from the surrounding, undisturbed area. The identification of the shear zones was achieved here in a rather primitive fashion. There are basically two shear zones, one to the west and a second to the east of Jutulstraumen which demarcate its margins. The width and margins of the shear zones can best be defined from satellite images. We used information supplied by Ole Anders Nøst, that the ice thickness grid has missing data values in these areas, which could not be reached due to the dangerous crevasse pattern of the shear zones. This results in wide shear zones on both sides of Jutulstraumen. Their shapes have been chosen as shown in Fig. 10 in dark red. In a next step, the ice thickness grid was used for another definition of the shear zones. The shear zones were defined towards Jutulstraumen along the gradient of the ice thickness distribution and with a small width. The width was chosen arbitrarily, but small. These second shear zones can be seen in Fig. 10 in blue colour.

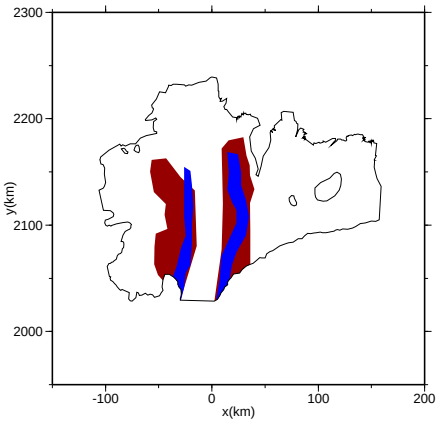

Figure 10: Definitions of shear zones. For further explanaition see main text.

E_s inside the shear zones is supposed to be extremly small, so that large velocities are reached. The set of enhancement factors inside and outside the shear zones was highly varied, although limited by the computation time. E_{ssz} is the value of E_s inside the shear zone and E_s denotes now the stress enhancement factor outside the shear zones. E_{ssz} was set equal to 0.1 and 0.01 and E_s varied from 1.0 to 0.15. In order to assure that enough nodes of the finite element grid are inside the shear zone, the number of additional nodes was increased dramatically, on cost of the computation time. Simulations were run with both kind of shear zones, that can however not all be shown here.

Wide Shear Zone We show only the runs with the ideal combination of E_s and E_{ssz} , that is when best agreement between computed and measured velocity at S1 is reached. Figure 11(left panel) shows the result for $E_s = 0.22$ and $E_{ssz} = 0.1$, with a speed at S1 of $721\,\mathrm{ma}^{-1}$.

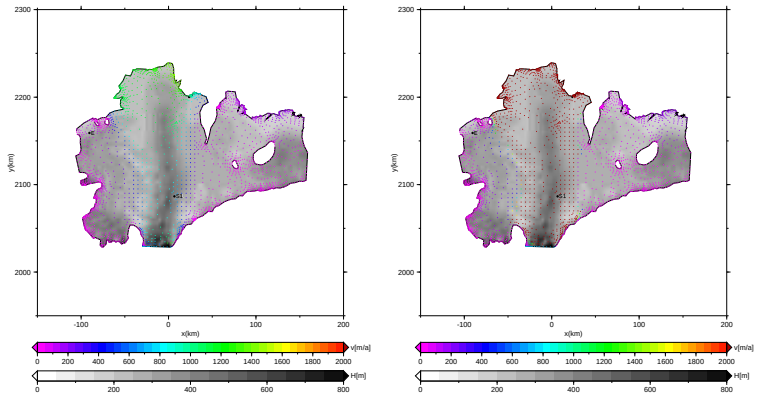

Figure 11: Horizontal velocity distribution using wide shear zones with $E_s = 0.22$ and $E_{ssz} = 0.1$(left panel) and $E_{ssz} = 0.01$(right panel). The colour denotes the magnitude of the velocity. More setup details: Ice thickness grid 'AWI', S1-like temperature profile and nonzero inflow.

Setting $E_{ssz} = 0.01$, the velocity at S1 increases to $819\,\mathrm{ma}^{-1}$. The whole structure of the horizontal velocity distribution changes toward an extremely fast inner part as can be seen in Fig. 11(right panel).

In order to monitor the changes both in the middle of the ice shelf and at the ice front, we define two other locations: one is the E-Base whilst a second one is a location directly at the ice front in the middle of Trolltunga. Table 1 (left panel) shows the speeds at these three locations for various parameter combinations. One conclusion is that the dominant parameter is the stress enhancement factor inside the shear zones. This confirms our expectation. On the other hand, the only realistic parameter combination is a combination with only a small difference between the stress enhancement factors inside and outside the shear zones. Furthermore, the ratio between the speed at S1 and at the ice front is increased to roughly one half with $E_{ssz} = 0.1$ to almost one with $E_{ssz} = 0.01$ (realistic is 720/2000=0.36). This means that the distribution of the horizontal velocity looses its characteristic structure of enhancement due to thinning.This unsatisfying result led us to run simulations with shear zones that are narrow.

Narrow Shear Zone For the simulations shown in this paragraph we used a narrow shear zone as shown in Fig. 10. The ideal set of stress enhancement factors turned out to be $E_s = 0.16$ and $E_{ssz} = 0.1$. The corresponding results can be seen in Fig. 12(left panel). The general structure of the velocity field is represented very well. However, the difference between E_s and E_{ssz} is again small; so we conclude that the narrow shear zone does not push the parameters in the direction we had hoped for. In contrast to the case with the wide shear zones, the value of E_s takes a value of E_s similar to that without shear zones.

Investigations of the role of E_{ssz} in the narrow shear zones were also carried out. The speeds of these runs are collected in Tab. 1 (right panel). The ratio of the speeds at S1 between $E_{ssz} = 0.1$ and 0.01 for the wide shear zones is 8.3×10^{-2} and decreases for the narrow shear zones down to 1.9×10^{-1}.

6 Conclusion and Outlook

The simulations show two edged result: with a temperature profile typical for melting, simulations can reach agreement with measurements by using of realistic values for the enhancement factor and even more so, with an enhancement factor that is close to that obtained on the Ross Ice Shelf (Humbert et al., 2005). This means, that the constitution of the ice has similarities, with, or at least does not differ too much from, the Ross Ice Shelf. On the other hand, simulations with an approximation to the measured temperature profile, that are supposed to be most realistic, can only reach agreement with measured horizontal velocities, when the stress enhancement factor is set equal to an unrealistically low value. One possibility to understand this result is that the measured temperature profile is not likely to be representative for the whole ice shelf. Of course, the processes on the ice/ocean interface are complex and the accumulation process might vary even at small scales. This could be tested using mixed areas of temperature profiles. In future, possibly, this could be achieved by using results from the ocean simulation of Ole Anders Nøst, similar to what was done

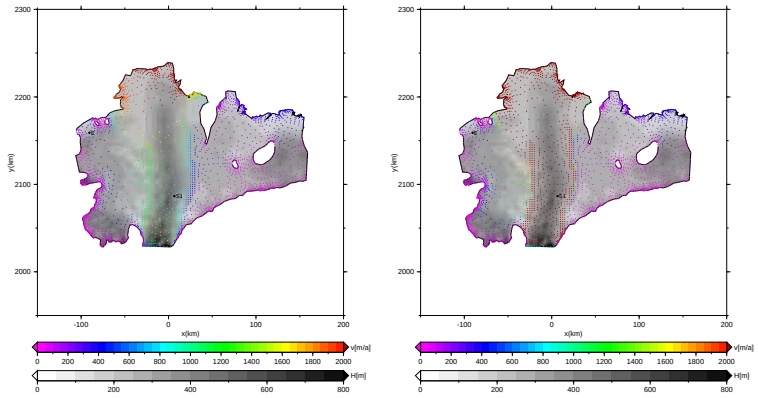

Figure 12: Horizontal velocity distribution using narrow shear zones with $E_s = 0.22$ and $E_{ssz} = 0.1$(left panel) and $E_{ssz} = 0.01$(right panel). The colour denotes the magnitude of the velocity. More setup details: Ice thickness grid 'AWI', S1-like temperature profile and nonzero inflow.

Table 1: Influence of the magnitude of E_{ssz} : Speeds (ma^{-1}) at three characteristic positions obtained by using narrow shear zones (left table) and wide shear zones (right table).

E_s	E_{ssz}	v@S1	v@E-Base	v@Trolltunga
0.2	0.1	819	150	1553
0.3	0.1	492	44	713
0.4	0.1	356	19	443
0.5	0.1	284	10	331
0.6	0.1	221	5	243
0.2	0.01	9834	129	9529
0.3	0.01	4903	28	4570
0.4	0.01	2663	14	2228
0.5	0.01	1863	10	1572
0.6	0.01	1196	4	965
Observed		720	—	—

E_s	E_{ssz}	v@S1	v@E-Base	v@Trolltunga
0.16	0.01	4612	282	5292
0.16	0.02	2549	308	3404
0.16	0.03	2573	332	3234
0.16	0.04	1800	337	2833
0.16	0.05	1434	343	2601
0.16	0.06	1217	338	2423
0.16	0.07	1095	339	2348
0.16	0.08	996	340	2285
0.16	0.09	917	340	2234
0.16	0.1	854	339	2188
Observed		720	—	—

for the Ross Ice Shelf (Humbert, 2005).
The role of the shear zones has so far only been tested in the context of an S1-like temperature profile. It would be valuable to intensify the study of shear zones also with other temperature profile parameterisations.

These conclusions pertain to the results obtained by our computations. They indicate that the available data allowing verification of the model equations are in this case insufficient. Indeed, an adequate parametrization of the depth integrated effective viscosity (a quantity needed in the theory and sensitive to the temperature distribution within the entire ice shelf) requires knowledge of the temperature distribution throughout the entire ice shelf. This is more than field glaciologists are able to provide at the moment. Therefore, basal meltrate distributions determined from ocean models should be used in future either to solve the temperature equation or to solve the temperature functions derived by Zotikov (1986).

Acknowledgements

Thanks are due to Ole Anders Nøst and Elisabeth Isaksson, Norsk Polar Institut, Tromsø, for the ice thickness data used in the simulations, the grounding line and for general support and exchange. Thanks are also due to Uwe Nixdorff and Daniel Steinhage from the Alfred Wegener Institute, Bremerhaven, for providing the ice thickness data of their airborne radio echo soundings.
On the evaluation of surface velocity data, we were kindly supported by numerous persons. Thanks are due to the 43rd SANAE overwintering team for their support in searching for velocity measurements of past teams on SANAE III, in particular Beneke de Wet and Pieter Wolmarans. Thanks are also due to Carol Jacobs, South African National Antarctic Program, South Africa and Jon P.S. Rash, University of KwaZulu-Natal, South Africa.

References

Craven, M., Elcheikh, A., Brand, R., and Allison, I., 2003. Hot water driling on the Amery Ice Shelf, East Antarctica. *Filchner-Rønne Ice Shelf Programme (FRISP), Report*, **14**.

du Plessis, A., 1973. Temperature Profiles Obtained from Boreholes on the Ice Shelf in the Vicinity of Sanae, western Dronning Maud Land. *S. Afr.Journal of Antarctic Research*, (3):11–15.

Fujino, K., Lewis, E. L., and Perkin, R. G., 1974. The Freezing Point of Seawater at Pressures up to 100 Bars. *Journal of Geophysical research*, **79** (12):1792–97.

Hooke, R. L., 1981. Flow Law for Polycrystalline Ice in Glaciers: Comparison of Therretical Predictions, Laboratory Data, and Field Measurements. *Reviews of Geophysics and Space Physics*, **19** (4):664–672.

Humbert, A., 2005. *Simulations of the Flow of the Ross Ice Shelf, Antarctica: parameter sensitivity tests and temperature-dependent ratefactor*. Department of Mechanics, Darmstadt University of Technology. ISBN 3-945868-10-3.

Humbert, A., Greve, R., and Hutter, K., 2005. Parameter sensitivity studies for the ice flow of the Ross Ice Shelf, Antarctica. *Journal of Geophysical Research, in print*, **110(F4)** (F04022):doi: 10.1029/2004JF000170.

Lunde, T., 1961. Snow accumulation in Dronning Maud Land . *Norsk Polarinstitutt. Skrifter.*:1–48.

Melvold, K., Hagen, J. O., Laumann, T., and Rolstad, C., 1997. Mass balance and dynamics on Jutulstraumen ice stream, NARE 1996/97. *Norsk Polarinstitutt. Meddelelser*, **148**:118–124.

Nøst, O. A., 2004. Measurements of ice thickness and seabed topography under the Fimbul Ice Shelf, Dronning Maud Land. *Journal of Geophysical Research*, **109** (C10010):doi:10.1029/2004JC002277.

Nøst, O. A. and Foldvik, A., 1994. A model of ice shelf-ocean interaction with application to the Filchner-Rønne and Ross Ice Shelf. *Journal of Geophysical Research*, **99** (C7):14,243–14,254.

Nøst, O. A., Goodwin, H., Rønstad, T., and Thorsen, S. H., 2002. Measuring the ice shelf draft and seabed topography below Fimbulisen. *Norsk Polarinstitutt. Meddelser*, **120**:30–37.

Orheim, O., Hagen, J. O., and Østerhus, S., 1990a. Studies on, and underneath, the ice shelf Fimbulisen. *Norsk Polarinstitutt. Meddelser*, **113**:59–73.

Orheim, O., Hagen, J. O., Østerhus, S., and Sætrang, A. C., 1990b. Glaciologic and oceanographic studies on Fimbulisen during NARE 1989/90 . *Filchner-Rønne Ice Shelf Programme (FRISP), Report*, **4**:120–131.

Orheim, O. and Lucchitta, B. K., 1987. Snow and Ice Studies by Thematic Mapper and Multispectral Scanner Landsat Images. *Annals of Glaciology*, **9**:109–118.

Paterson, W. S. B., 1994. *The Physics of Glaciers*. Pergamon Press, Oxford, 3rd edition.

Steinhage, D., Nixdorf, U., Meyer, U., and Miller, H., 1999. New maps of the ice thickness and subglacial topography in Dronning Maud Land, Antarctica, determined by means of radio-echo sounding. *Annals of Glaciology*, **29**:267–272.

Swithinbank, C. W. M., 1957. The regime of the ice shelf at Maudheim as shown by stake measurements . *Norwegian-British-Swedish Antarctic Expedition, 1949-52. Scientific results. Glaciology I., Norsk Polarinstitutt*, **3**:41–75,.

Weis, M., 2001. *Theory of shallow ice shelves and numerical implementation*. Ph.D. thesis, Institut für Mechanik AGIII, Technische Universität Darmstadt, Germany.

Weis, M., Greve, R., and Hutter, K., 1999. Theory of Shallow Ice Shelves. *Continuum Mechanics and Thermodynamics*, **11**:11–50.

Zotikov, I. A., 1979. Antifreeze-thermodrilling for core through the central part of the Ross Ice Shelf (J-9 Camp), Antarctica. *CRREL Report*, **79-24**:1–12.

Zotikov, I. A., 1986. *The thermophysics of glaciers*. D. Reidel Publishing Company.

Zotikov, I. A., Zagorodnov, V. S., and Raykovskiy, Y. V., 1980. Core drilling through the Ross Ice Shelf (Antarctica) confirmed basal freezing . *Science*, **207** (4438):1463–1465.